Composites Science and Technology 182 (2019) 107782

Contents lists available at ScienceDirect

Composites Science and Technology

journal homepage: www.elsevier.com/locate/compscitech

Conductive shear thickening gel/Kevlar wearable fabrics: A flexible body armor with mechano-electric coupling ballistic performance

Chunyu Zhao[a], Yunpeng Wang[a], Saisai Cao[a], Shouhu Xuan[a,**], Wanquan Jiang[b], Xinglong Gong[a,*]

[a] CAS Key Laboratory of Mechanical Behavior and Design of Materials, Department of Modern Mechanics, CAS Center for Excellence in Complex System Mechanics, University of Science and Technology of China, Hefei, Anhui, 230027, China

[b] Department of Chemistry, University of Science and Technology of China, Hefei, 230026, PR China

ARTICLE INFO

Keywords:
Kevlar fabrics
Anti-impact behavior
Mechano-sensing behavior
Shear thickening gel

ABSTRACT

This work reported a novel conductive shear thickening gel-Kevlar fabrics (c-STG/Kevlar) body armor material which possessed both anti-impact performance and dynamic mechano-sensing behavior. Due to the excellent shear thickening effect, the c-STG/Kevlar showed a higher safeguarding property than the neat Kevlar. Under low-velocity drop tower loading, the maximum center force of c-STG/Kevlar was only 5768 N, which was nearly half of the neat Kevlar (11414 N). During the high-velocity ballistic testing, the monolayer c-STG/Kevlar sample could absorb 21.6% impact energy. The c-STG/Kevlar displayed a mechano-electric coupling character since the electrical resistance of the c-STG/Kevlar was linearly dependent on the external impacts. A possible sensing mechanism was proposed and it was found that the impact damages could be evaluated by the resistance variation. Finally, an *in situ* impact-sensing helmet was obtained by using c-STG/Kevlar, which indicated that the above smart fabrics had wide potential in next generation body armor materials and wearable devices.

1. Introduction

During the human social life, the development of high performance protective materials, espacially the body armor, has attracted wide interests due to the complex international situation, regional conflicts, and frequent terrorist activities. The original body armor was always fabricated by heavy materials, such as metals [1], aluminum alloys [2,3], ceramic reinforced composites [4,5], and high strength glass [6,7], etc. However, most of these hard materials were inconvenient to wear and significantly limitated human's activities. Nowdays, multilayer aramid fabrics were applied to produce flexible body armors, because they were much lighter, softer and more comfortable than the previous hard bulletproof materials [8,9]. To further enhance the anti-impact performance, several methods have been developed on modifying the aramid fabrics. Both the experimental and theoretical results indicated that introducing nanohybrids into the fabrics could not only improve the friction between fabrics yarns but also enhance the ballistic impact resistance [10–13]. To this end, many efforts have been done to develop multi-component aramid fabrics toward high performance soft body armor.

Shear thickening materials, whose mechanical properties could be sthrengthened while encountering the unexpected impact, have been proven to be wonderful candidates for improving the anti-impact performance of aramid fabrics while keeping the desirable flexible characteristic [14–16]. Since Wagner [17] firstly developed the shear thickening fluid/Kevlar (STF/Kevlar) body armor, numerous comtribution were emeraged in studying the energy adsorption mechanism of the STF/Kevlar [18–21]. All the stab resistant testing [22,23], Split-Hopkinson pressure bar (SHPB) testing [24], hypervelocity impact testing [25–27] clearly illustrated that the impact resistance of the STF/Kevlar composites was effectively enhanced by the improving friction and shear thickening effect. Unfortunately, the stability and sealing problem limited the further application of STF/Kevlar. Recently, it was found that the mechanical properties of STF/Kevlar could be enhanced by covering a shear thickening gel (STG) layer [28]. The synergestic shear thickening effect between the STF and STG increased the anti-impact performance. Furthermore, the STG sandwiched between two Kevlar layers exhibited better energy dissipation performance during the high-speed impact, which proved the borad potential of the STG in soft body armor [29,30]. However, the detailed anti-impact performance of the STG/Kelvar fabrics has not been carefully investigated.

Besides resisting the mechanical impact, the coming-generation soft body armor is also required to be sensitive to the external simulus. *In situ* monitering the impact quantity and location during the external

* Corresponding author.
** Corresponding author.
E-mail addresses: xuansh@ustc.edu.cn (S. Xuan), gongxl@ustc.edu.cn (X. Gong).

https://doi.org/10.1016/j.compscitech.2019.107782
Received 4 April 2019; Received in revised form 6 August 2019; Accepted 12 August 2019
Available online 13 August 2019

loading become a necessary advantage in modern safe-guardening. As an important member of the smart wearable devices, the multi-component Kevlar fabrics with mechano-electric coupling property is urgently required in soft body armor. Previous studies illustrated that electronic fabrics with good electrical properties could be obtained by introducing conductive media into the fabrics [31]. Moreover, owning to the gel-like structure, multifunctional STG with magnetic or electric character could be very easily achieved [32,33]. It was reported that the PU sponge incorporated with conductive STG (c-STG) showed interesting sensing behvior to the external impact [34]. Due to the mechano-electric coupling character, the PU/c-STG could even dynamically detect the motion degree of the joints. Our recent results indicated that the STG/CNT/Kevlar multi-layer fabrics could monitor the fingers and elbow bending beyond safe-guardening fabrics [35]. As a smart body armor, simulteneously detecting the hypervelocity impact damage is a key parameter for its practical applications. Nevertheless, due to the lack of STG/Kelvar fabrics, the dynamic mechano-electric coupling properties of soft body armor, especially in the ballistic condition, has not been investigated.

In this work, a flexible body armor composite was fabricated by impregnating carbon black filled conductive STG (c-STG) into Kevlar fabrics. Both the low- and high-velocity impact testing indicated that the anti-impact properties of c-STG/Kevlar were reinforced by c-STG. Owing to the conductive carbon black, the c-STG/Kevlar showed a typical mechano-electric coupling behavior. The electrical conductivity of the c-STG/Kevlar displayed a simulteneous response to ballistic impacts and the detailed mechanism was disscussed. Finally, a self-sensing anti-impact helmet based on the c-STG/Kevlar was constructed and it could not only resist the external impact but also effectively monitor the destructiveness through the dynamic changes of resistance.

2. Materials and methods

2.1. Materials

Boric acid (Sinopharm Chemical Reagent Co. Ltd, Shanghai, China), hydroxyl silicone oil (500 mm^2/s, AR degree, from Jining Huakai Resin Co. Ltd) were raw materials to synthesize STG. Carbon black (Product type: VXC-72, from Cabot Corporation, Boston, Massachusetts, USA) was conductive filling material. Acetone (Sinopharm Chemical Reagent Co. Ltd, Shanghai, China) was the solvent to dissolve the STG. Kevlar fabrics were provided from Junantai Protection Technologies Co. Ltd, Beijing, China.

2.2. Preparation of c-STG/Kevlar wearable fabrics

Firstly, the boric acid and hydroxyl silicone oil (mass ratio 1:20) were mixed and heated at 180 °C for 2 h. Secondly, the mixture was cooled down to room temperature and the raw STG polymer was obtained. Then, the raw STG polymer and carbon black was dissolved in the acetone to achieve a homogeneous solution. Next, the Kevlar fabrics were immersed in the above conductive STG (c-STG) solution and dryed in an oven. Finally, the c-STG/Kevlar fabrics with different STG content were fabricated by repeating the abovementioned dissolution-volatilization progress (Fig. 1). For simplicity, the definition and the specific parameters of the samples were shown in Table 1.

Table 1
The definition and parameters of samples.

Name (abbreviation)	Mass Ratio			Areal Density of Monolayer ($kg \cdot m^{-2}$)
	Carbon black	STG	Kevlar	
Sample 1 (S1)	0	0	1	0.200
Sample 2 (S2)	0	0.200	1	0.258
Sample 3 (S3)	0	0.400	1	0.294
Sample 4 (S4)	0	0.600	1	0.323
Sample 5 (S5)	0	0.800	1	0.375
Sample 6 (S6)	0.025	0.600	1	0.323
Sample 7 (S7)	0.050	0.600	1	0.336
Sample 8 (S8)	0.075	0.600	1	0.345
Sample 9 (S9)	0.025	0.575	1	0.321
Sample 10 (S10)	0.050	0.550	1	0.321
Sample 11 (S11)	0.075	0.525	1	0.319
Sample 12 (S12)	0.100	0.500	1	0.320

2.3. Characterization and statics testing

A digital camera (Nikon D7000) and the SEM (FEI, type: XL-30ESEM) were used to observe the macroscopic and microscopic morphologies of Kevlar and c-STG/Kevlar. The rheological properties of the STG and c-STG composite were investigated by a rheometer (Physica MCR 302, Anton Paar Co., Austria). Frequency sweeping testing was carried out with a PP20 parallel plate (Φ20 mm) and the dimension of the specimens was Φ20 mm×1 mm. During the rheological testing, the frequency swept from 0.1 Hz to 100 Hz with a strain of 1% at the temperature of 25 °C. The yarn pull-out testing of monolayer fabrics was conducted on MTS tensile testing machine (MTS Criterion ™ Model 43) to analyze the friction effect. The intermediate yarn was selected as the pull-out end, then the outstretched portions of the yarns were fixed. Therefore, the intermediate yarn could be pulled out following the chuck movement. The signals of pull-out force and displacement were collected by the MTS force sensor. In this testing, the pull-out end velocity was set as 50, 150 and 300 mm/min.

2.4. Low-velocity drop tower impact testing

The low-velocity impact drop tower testing system (Fig. 2a and d) was made up of a drop tower testing device (ZCJ1302-A, MTS Co. Ltd, China), a force sensor and a dynamic signal test and analysis system (DH5920N, Donghua Testing Technology Co., Ltd, Jiangsu, China). A 2.0 kg standard impactor with a diameter of 25 mm and a knife impactor (Fig. 2c) were chosen to investigate both non-penetrating and penetrating process of the samples. The standard impactor dropped from specific heights and struck the target consisted of the samples, the 2 cm thick neoprene sponges and the force sensor located in the center of the base (Fig. 2b). The impact force signals were collected simultaneously by the dynamic signal test and the analysis system during the impact process. When the knife impactor was used, the witness paper

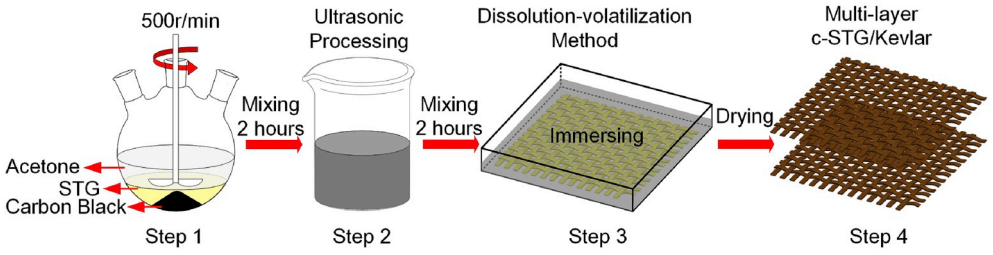

Fig. 1. The schematic of the dissolution-volatilization method to prepare multi-layer c-STG/Kevlar composite.

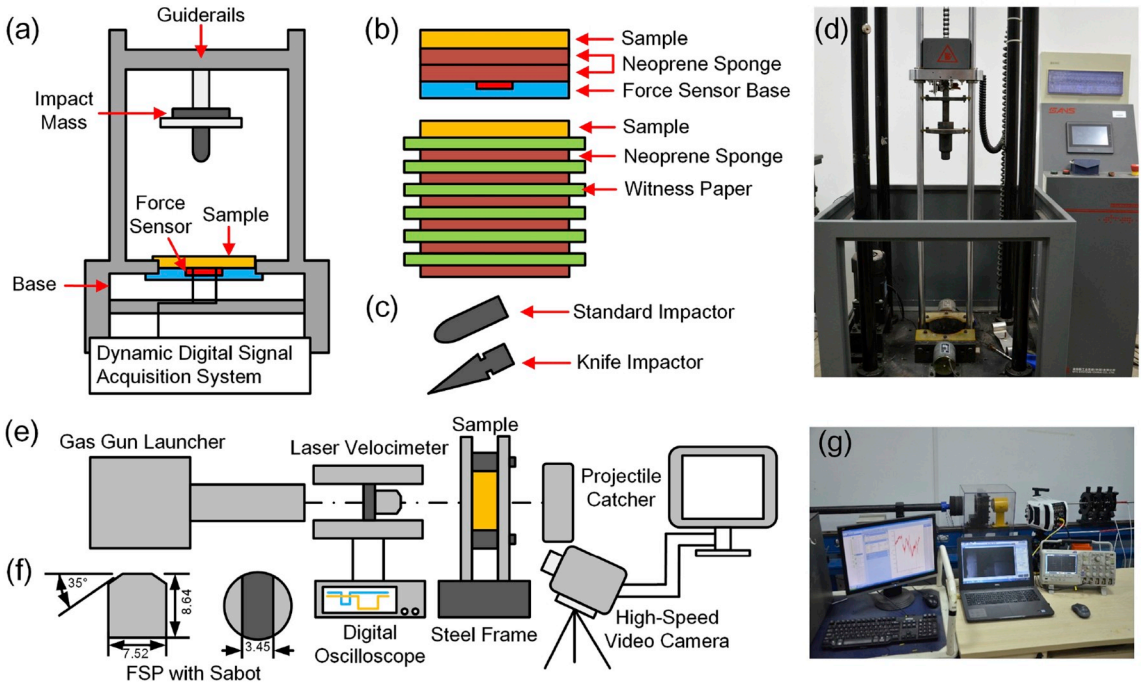

Fig. 2. (a–d) The schematic and device images of the low-velocity drop tower impact testing; (e–g) the schematic and device images of the high-velocity ballistic impact testing.

was attached on the surface of each layer of fabrics composites (Fig. 2b), and the penetration layers were recorded to measure the destruction level. In particular, the target was fixed by the rubber rings and it could be considered as a state of free boundary condition.

2.5. High-velocity ballistic impact testing

The high-velocity experimental system was comprised of a gas gun as the launcher, a laser speedometer to measure the impact velocity of the projectile, the projectile with a sabot, a steel frame fixed with the target, and a high-speed video camera. According to the NIJ Standard 0101.04 and MIL-DTL-46593B, a 44 grain (2.85 g) chisel-nosed steel fragment simulating projectiles (FSP) was used (Fig. 2e–g). In this experiment, the velocity of the projectile was controlled from 55 m/s to 160 m/s. The sample was mounted on a frame with clamping boundary conditions. In addition, the high-speed video camera (Phantom v2512,Vision Research Inc.) was used to capture the morphology of samples and record the trajectory of the FSP. The samples were placed approximately 15 cm away from the muzzle so that the yaw and velocity decay of the FSP could be neglected.

3. Results and discussion

3.1. Preparation and characterization of c-STG/Kevlar soft fabrics

The c-STG/Kevlar was obtained by incorporating c-STG into the Kevlar fabrics. Firstly, the pure STG synthesized according to our reported method showed a typical shear thickening behavior and the storage modulus could increase from 381 Pa to 530 kPa when the shear frequency scanned from 0.1 Hz to 100 Hz, respectively (Fig. 3a). After doping the conductive carbon black, the c-STG was achieved. With increasing the content of carbon black, both the minimum storage modulus (G'_{min}) and maximum storage modulus (G'_{max}) of the c-STG were increased, which must be responded for the particle-strengthening effect (Fig. 3a). Althought the relative shear thickening effect decreased, the $\Delta G'(G'_{max} - G'_{min})$ increased with the carbon black content (Fig. 3b).

The microscopic and macroscopic morphologies of the neat Kevlar and c-STG/Kevlar were investigated. As shown in Fig. 4a was the SEM image of the neat Kevlar. It was very clear that the Kevlar fabric was composed of fibers and there were obvious gaps between the fibers. After immersing the c-STG, the gaps were fullfilled and the c-STG/Kevlar hybrid fabrics were constructed (Fig. 4b). Because the c-STG was black which was originated from the carbon black, the Kevlar transformed from yellow to black after the immersing treatment (Fig. 4c and d). The macroscopic images indicated the c-STG was homogeneously dispersed in the Kevlar fabrics.

The c-STG improved the internal friction between the fibers, which could be qualitatively analyzed by yarns pull-out testing conducted on MTS tensile testing machine (Fig. 5a). As shown in Fig. 5b–d, three states were found in the pull-out testing process. Firstly, the yarns were slack in the initial state and the pull-out force (F_p) value was 0 N. Once yarns started to move, F_p swiftly reached the peak value because of the instantaneous friction caused by the relative motion of yarns. Secondly, the F_p declined with fluctuation since the reduction of contacting area between the pull-out end and the surrounding fabrics. Finally, the F_p decreased to 0 N when the yarns were completely pulled out.

For the neat Kevlar S1, the maximum values of pull-out force ($F_{p\text{-}max}$) under different pull-out velocity were 1.8 N, 1.7 N, 1.9 N (Fig. 5b). There was no obvious distinction for $F_{p\text{-}max}$ which illustrated that the neat Kevlar was not a sort of rate-dependent material. However, for the STG/Kevlar S4 (STG:Kevlar = 0.6:1), the $F_{p\text{-}max}$ gradually improved as the pull-out velocity increased (Fig. 5c). The $F_{p\text{-}max}$ value was only 6.9 N at the pull-out velocity of 50 mm/min, and it reached to 10.9 N (150 mm/min) and 14.8 N (300 mm/min). As we know, the mechanical property of the STG was dependent on the external loading and altered by the shear rate. After adding the STG into Kevlar, the interaction between the Kevlar yarns was increased. With increasing of the pull-out velocity, the shear thickening effect happened thus the STG/Kevlar displayed a rate-dependent behavior.

Moreover, our above analysis indicated the c-STG showed larger $\Delta G'$ than the STG. Therefore, when the carbon black particles doped c-STG was used to form the c-STG/Kevlar, the $F_{p\text{-}max}$ was further improved. The $F_{p\text{-}max}$ of S7 c-STG/Kevlar fabrics (carbon black:STG:Kevlar = 0.05:0.6:1) increased from 11.9 N to 16.6 N, 19.7 N

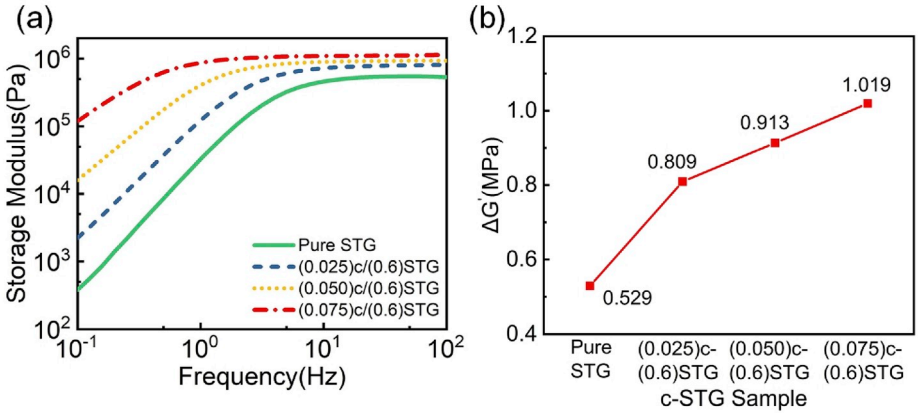

Fig. 3. Rheological testing: (a) the curve of storage modulus of samples *vs* frequency; (b) the $\Delta G'$ of samples. (mass ratio of STG *vs* Kevlar fabrics fixed at 0.6, changing the mass ratio of carbon black *vs* Kevlar at 0.025, 0.05 and 0.075, respectively).

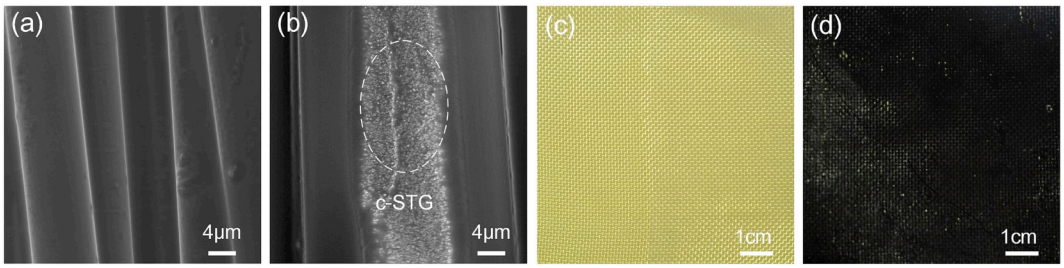

Fig. 4. The microscopic SEM morphological images of (a) neat Kevlar and (b) c-STG/Kevlar samples; the macroscopic images of (c) neat Kevlar and (d) c-STG/Kevlar samples.

with the growing pull-out velocity owing to the friction reinforcement resulted from better shear thickening property of c-STG (Fig. 5d). Obviously, during the pull-out process, the conductive carbon black particles showed reinforcement performance on the mechanical property of the final c-STG/Kevlar. The partical strenthening effect and shear thickening property worked synergistically to resist the yarns

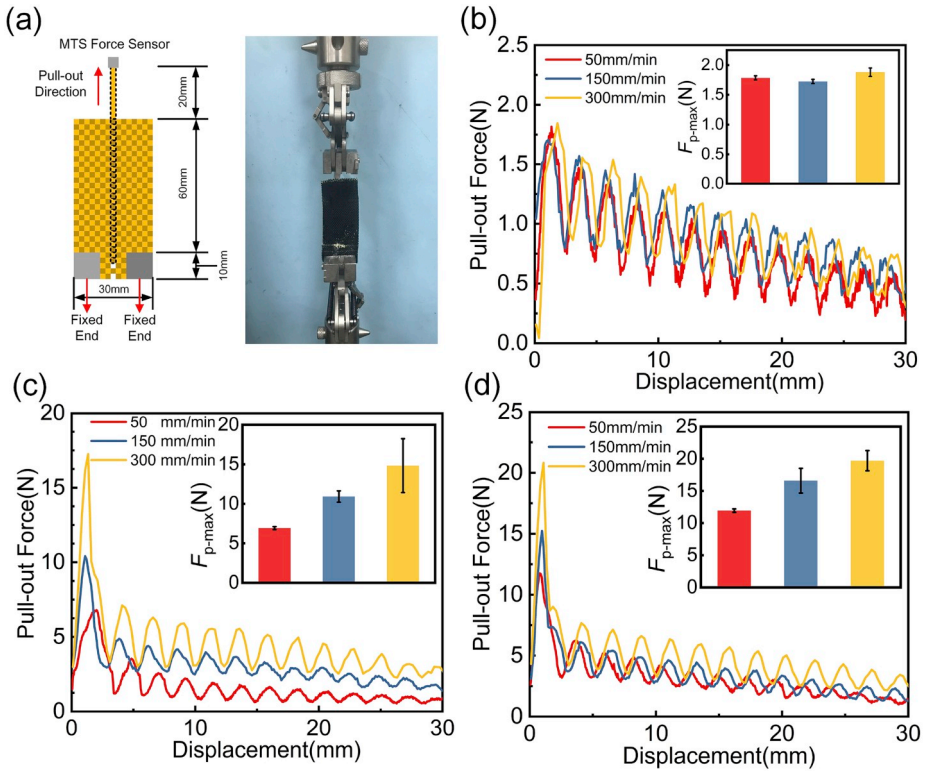

Fig. 5. (a) The schematic of the size of the sample during the yarn pull-out testing and the image of the MTS tensile testing machine device; the typical curve of pull-out force *vs* the displacement: (b) neat Kevlar; (c) S4 STG/Kevlar; (d) S7 c-STG/Kevlar. (inset bar graphs represented the maximum pull-out force $F_{p\text{-}max}$).

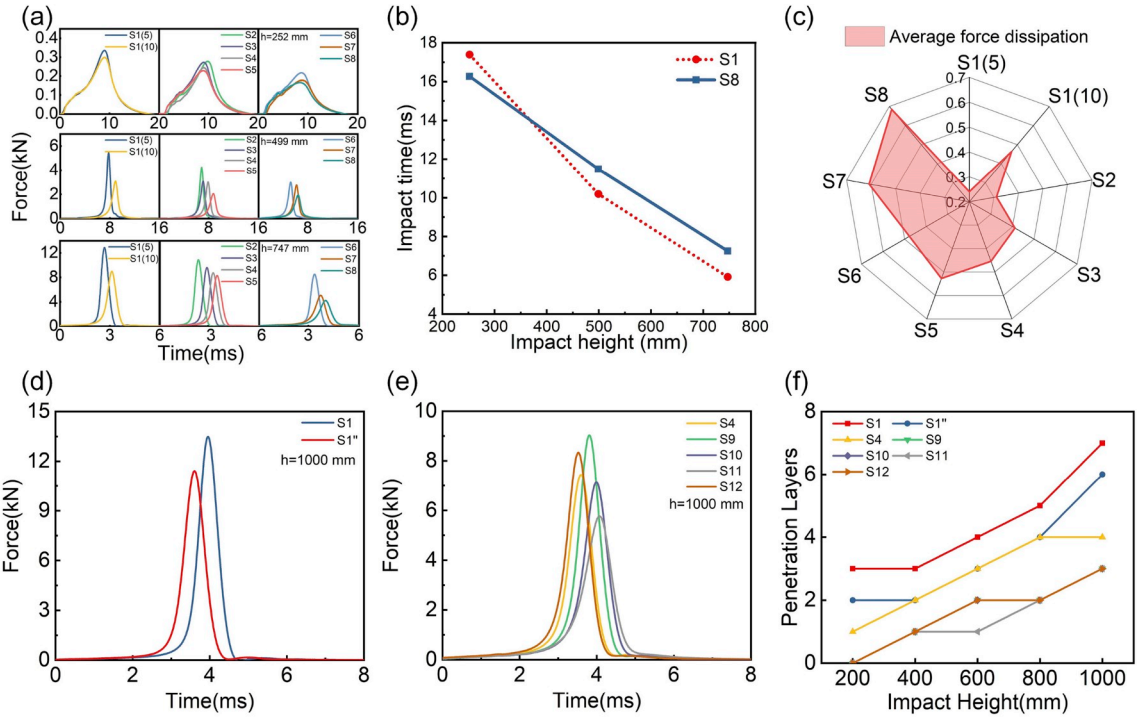

Fig. 6. Low-velocity impact: (a) the curve of center impact force *vs* time of standard impactor at different impact heights; (b) the impact time of 5 layer c-STG/Kevlar (S8) and 5 layer neat Kevlar (S1) at different impact heights; (c) the average impact force dissipation rate of the samples; (S1(5) and S1(10) represented for the 5-layer S1 and 10-layer S1, respectively); The curve of center impact force *vs* time of standard impactor at the impact height of 1000 mm: (d) neat Kevlar; (e) coupling c-STG/Kevlar; (S1(15) and S1(24) represented for the 15-layer S1 and 24-layer S1, respectively) (f) the curve of center penetration layers *vs* impact height of knife impactor end at different impact heights. (The curves of sample S9, S10 and S12 coincide.)

deformation which enhanced mechanical properties of the fabrics.

3.2. Anti-impact mechanical performance of c-STG/Kevlar soft fabrics

The anti-impact property was a significant indicator for the mechanical parameter of fabrics. In this section, low- and high-velocity impact properties were studied to discuss the safeguarding performance of c-STG/Kevlar. In the low-velocity impact testing, the standard impactor was released at specific heights to analyze the influence of filling materials on the anti-impact performance. For all of the samples, the force signals increased to the peak value ($F_{c\text{-}max}$) within a few milliseconds once the impactor contacted the surface (Fig. 6a and 6b). Firstly, the force-time curves of 5-layer and 10-layer neat Kevlar (S1), 5-layer STG/Kevlar (S2–S5) were compared (Fig. 6a). The $F_{c\text{-}max}$ decreased significantly as the growth of the mass ratio of STG since more STG was able to better resist impact due to the shear thickening properties. The STG inevitably reduced the flexibility of the Kevlar. Hence, in order to well combine the anti-impact resistance and the wearing flexibility, the mass ratio of STG to Kevlar was fixed to 0.6 for the following study.

Secondly, the curves of c-STG/Kevlar sample (S6–S8) indicated that the addition of reinforcing carbon black into the STG/Kevlar further improved the anti-impact performance. Similarly, the $F_{c\text{-}max}$ of the c-STG/Kevlar decreased with the growth of conductive carbon black content. Fig. S1 showed the $F_{c\text{-}max}$ for c-STG/Kevlars at different impact heights. It was noted that the 5-layer c-STG/Kevlar S8 with a smaller areal density had a better anti-impact property than the 10-layer neat Kevlar. For 10-layer Kevlar, the $F_{c\text{-}max}$ were 299 N (252 mm), 3130 N (499 mm), 8982 N (747 mm), respectively. However, the corresponding $F_{c\text{-}max}$ of 5-layer c-STG/Kevlar obviously decreased to 165 N (252 mm), 2215 N (499 mm), 4823 N (747 mm).

The average dissipation rate of impact force in the i sample $\eta_a(i)$ was calculated by the Eq. (1).

$$\eta_a(i) = \left(\sum_{j=1}^{3} \frac{F_{c-max}(i, h_j) - F_{c-max}(0, h_j)}{F_{c-max}(0, h_j)} \times 100\% \right) / 3 \quad (1)$$

The $F_{c-max}(i, h_j)$ and $F_{c-max}(0, h_j)$ corresponded to $F_{c\text{-}max}$ of i sample and the blank control group which was consisted of neoprene sponges at the number j height, respectively. The average impact force dissipation rate of c-STG/Kevlar (68.5% for S8) was larger than STG/Kevlar (45.5% for S4) and neat Kevlar (46.4% for 10-layer S1) with the similar areal density (Fig. 6c). This phenomenon demonstrated that appropriate c-STG not only improved the safe-guarding property but also saved the mass and thickness.

To maintain the softness and flexibility of the STG/Kevlar, it was necessary to study an optimal proportion of the carbon black in c-STG. Here, keeping the mass ratio of c-STG *vs* Kevlar at 0.6 (S4, S9–S12), the coupling relationship between carbon black and STG was studied. Primarily, the same stardard impactor testing was conducted at a height of 1000 mm to magnify the differences. The results manifested that all of the samples (15-layer S4, S9, S10, S11, and S12) exhibited better impact resistance than the 15-layer neat Kevlar and 24-layer neat Kevlar S1 with the same areal density (Fig. 6d). The 15-layer S4 (STG/Kevlar) showed a maximum of $F_{c\text{-}max}$ (13483 N) and the S11 (c-STG/Kevlar) possessed the minimum $F_{c\text{-}max}$ (5768 N) (Fig. 6e and Fig. S2). The results demonstrated that the S11 generated larger friction among the fibers to resist non-penetration destruction than the other samples during the loading process.

Then, the knife impactor loading testing was also conducted. Here, the impact height was set at 204 mm, 401 mm, 597 mm, 799 mm and 1017 mm, respectively. As shown in Fig. 6f, the penetration layers increased as the impact height increased. Clearly, all of the hybrid Kevlar samples had smaller penetration layers than the neat Kevlar. In this failure mode, the c-STG absorbed the energy prior to the fracture of fibers, which promoted the rigidity against the impact loading. The S11 also showed better penetration resistance effect than other samples

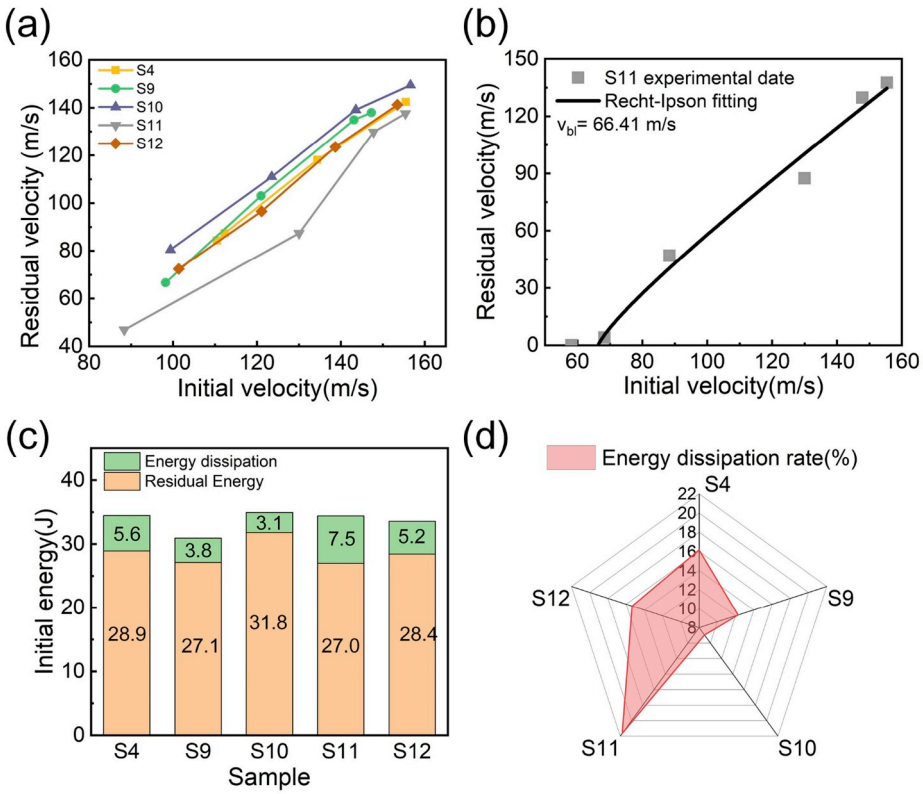

Fig. 7. High-velocity impact of coupling c-STG/Kevlar samples: (a) the curve of residual velocity *vs* initial velocity; (b) Rechit-Ipson fitting of the S11 c-STG/Kevlar sample; (c) bar diagram of energy information of different samples; (d) energy dissipation rate of different samples.

with relative smaller penetration layers. Therefore, by summarizing the results of the penetration and non-penetration low-velocity drop tower impact testing, the S11 exhibited the outstanding property against the external loading.

Moreover, the high-velocity ballistic testing was further conducted. The safeguarding performance of the c-STG/Kevlar could be acquired by studying the curves of initial velocity *vs* residual velocity. At a similar initial impact velocity, the S11 dissipated more impact energy with lower residual velocity than the other samples (Fig. 7a). The ballistic limit velocity (v_{bl}) was estimated by the modified Recht-Ipson method (Eq. (2)). The α, p and v_{bl} were pending parameters [36], v_{res} and v_{ini} corresponded to initial and residual velocity. The fitting result of the ballistic limit velocity v_{bl} of S11 was 66.41 m/s (Fig. 7b), which was well corresponded to the subsequent mechano-electric testing.

$$v_{res} = \alpha \times (v_{ini}^{p} - v_{bl}^{p})^{1/p} \tag{2}$$

$$E_{ini} = \frac{1}{2} \times m \times v_{ini}^{2} \; E_{res} = \frac{1}{2} \times m \times v_{res}^{2} \tag{3}$$

$$E_{dis} = E_{ini} - E_{res} = \frac{1}{2} \times m \times v_{ini}^{2} - \frac{1}{2} \times m \times v_{res}^{2}$$

$$\eta_{dis} = \frac{E_{dis}}{E_{ini}} \times 100\% = \frac{E_{ini} - E_{res}}{E_{ini}} \times 100\% \tag{4}$$

The energy absorption behavior was utilized to further discuss the excellent anti-impact performance of S11 according to Eq. (3) and Eq. (4). The $E_{ini}$and E_{res} corresponded to the initial and residual energy calculated by the Eq. (3). E_{dis} and η_{dis} represented the energy dissipation and energy dissipation rate, and m was the mass of the FSP, respectively. The high-velocity FSP could completely penetrate the sample in a very short time. As soon as the FSP contacted the surface of c-STG/Kevlar, the fabrics breakage suddenly occurred to resist against the impact. Meanwhile, the c-STG transformed into a tough solid-state to dissipated impact energy, owing to excellent shear thickening property. Similarly, the result clearly displayed that the S11 c-STG/Kevlar possessed the best energy dissipation ability. As shown in Fig. 7c was the results for S4, S9, S10, S11, S12 at the velocity around 150 m/s. The E_{dis} of S11 was 7.5 J, which was much larger than the S4 (5.6 J), S9 (3.8 J), S10 (3.1 J) and S12 (5.2 J). Furthermore, the energy dissipation rates for these samples were distinctively different. The energy dissipation rate of monolayer S11 sample was 21.6%, while the monolayer S10 showed only 9% (Fig. 7d). The apparent comparison result in energy dissipation performance proved that S11 possessed the best ability of absorbing impact energy.

Supplementary data related to this article can be found at https://doi.org/10.1016/j.compscitech.2019.107782.

The destruction features of morphologies for c-STG/Kevlar S11 and neat Kevlar S1 at the initial velocity of 68.3 m/s and 75.7 m/s were recorded integrallty by high-speed photography. Once the FSP reached the surface of the samples, the displacement of fabrics in the central region evolved from a point to a small pyramid. The morphology of the neat Kevlar showed the obvious macroscopical breakage of fibers after penetrating process (Fig. 8a and Movie S1). Due to the relatively weak friction between the fibers, it was difficult for the neat Kevlar to form an integral structure to resist the impact, and the uneven force between the fibers caused the FSP to deflect. Different from the neat Kevlar, the destruction area of S11 was much smaller and there was almost no significant vibration on the surface of c-STG/Kevlar (Fig. 8b and Movie S2). The S11 sample presented good structural stability and vibration isolation under the high-velocity impact. Obviously, the strong tension between the fibers resulting from the c-STG prevented deflection of the FSP trajectory.

Furthermore, the microstructure and macrostructure of the samples after the penetration process could reveal the anti-impact mechanism of the c-STG/Kevlar. For neat Kevlar, the overall damage of the material was derived from the fracture of every single fiber. There was almost no interaction force among the fibers and the energy for FSP to penetrate the sample was relatively small, which resulted in the smooth fracture

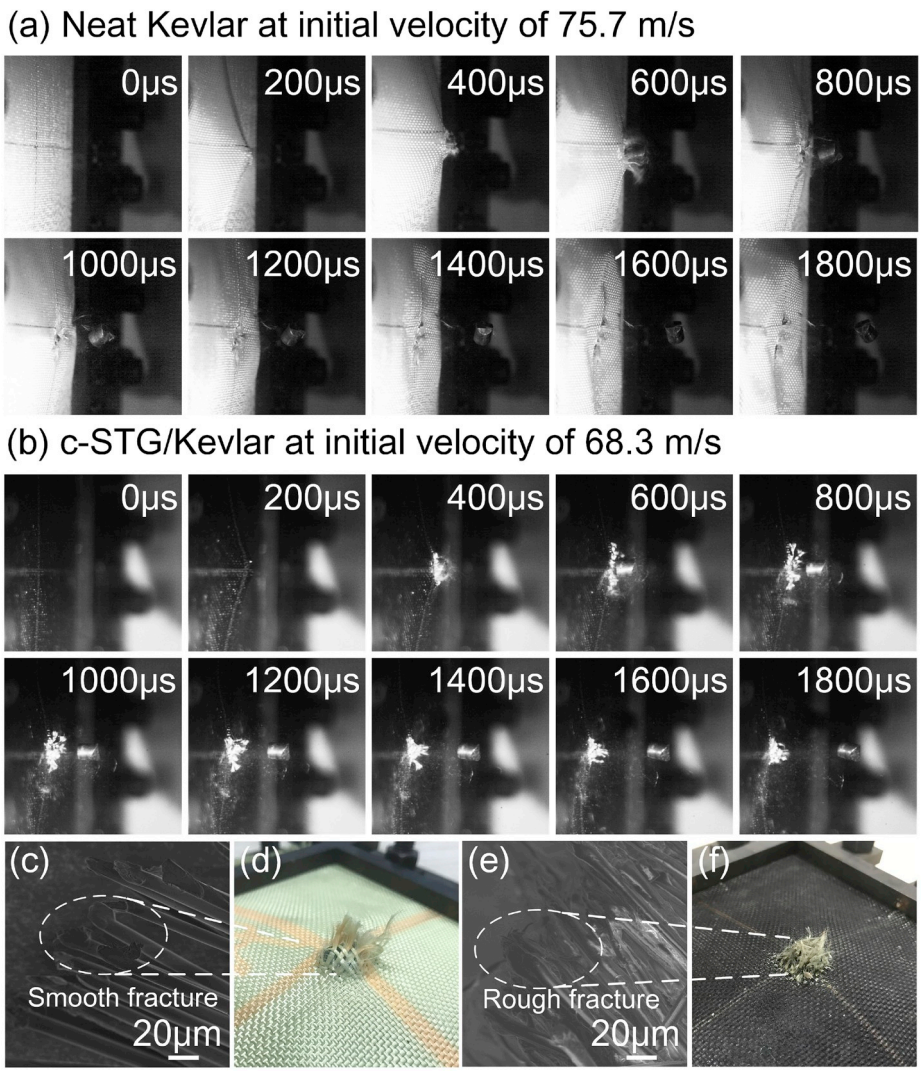

Fig. 8. The high-speed photography macroscopical images of (a) neat Kevlar S1 at initial velocity of 75.7 m/s; (b) c-STG/Kevlar S11 at initial velocity of 68.3 m/s during the impact testing process; (c) The SEM microstructure fracture and (d) the macroscopic fracture images of neat Kevlar S1 after the FSP penetration; (e) the SEM microstructure fracture and (f) the macroscopic fracture images of c-STG/Kevlar S11 after the FSP penetration.

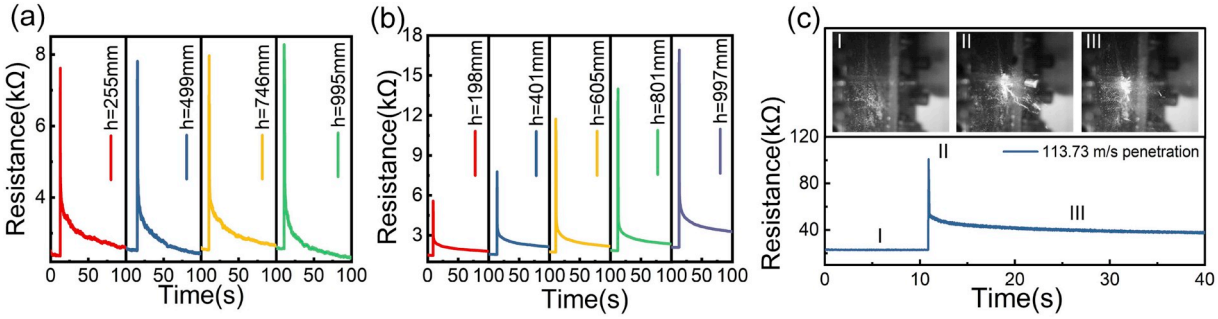

Fig. 9. The curves of the resistance signal of c-STG/Kevlar composites under (a) low-velocity standard impactor loading; (b) low-velocity knife impactor loading; (c) high-velocity penetration ballistic impact and the corresponding fabrics states.

of fibers (Fig. 8c and d). However, because of the excellent friction reinforcement and the shear thickening property of c-STG, the adhesion stress between the c-STG and Kevlar fibers was effectively promoted. Therefore, the failure mode transformed into general demolition of fabrics. In this case, the fracture of c-STG/Kevlar was rougher than neat Kevlar (Fig. 8e and f) which indicated that the FSP required more energy to penetrate the composite. Hence, the impact energy could be effectively dispersed for c-STG/Kevlar and the synergistic effect of c-STG and Kevlar fabrics got a better embodiment.

3.3. Mechano-electric coupling performance of c-STG/Kevlar soft fabrics

The reinforcing performance of c-STG/Kevlar was comprehensively studied by the above mechanical experiments. On account of the good conductivity of carbon black, the c-STG/Kevlar was expected to be conductive and its resistance would be responsive to the external stress.

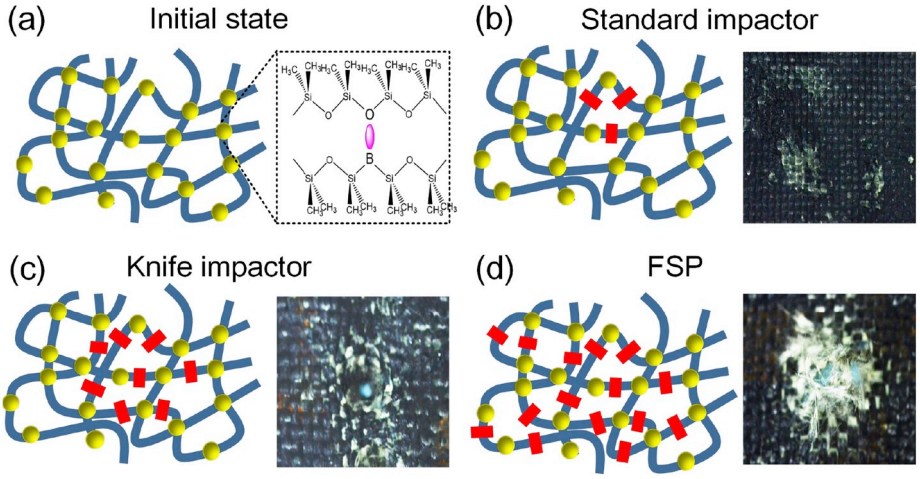

Fig. 10. Schematic of the mechanism explanation for mechano-electric performance.

In this work, the mechano-electric coupling performance of the c-STG/Kevlar S11 which possessed the best anti-impact property was also investigated. During the testing, different forms of impact were loaded on the c-STG/Kevlar. Simultaneously, the resistance variation of the composite was recorded by the electrochemical impedance spectra (EIS) system.

Firstly, the electric resistance variation of 5-layer S11 against drop tower impact was investigated through both standard and knife impactor (Fig. 9a and b). The initial resistance of S11 remained almost unchanged at around 2.0 kΩ, which further indicated that conductive c-STG was evenly distributed in the fabrics composites. During the impact process, the resistance of the S11 rapidly increased to the peak value as soon as the impactor contacted the surface of the fabrics. Moreover, the electric resistance of the S11 could recover to initial resistance in 40 s once the impact loading was completed, showed an excellent recoverable property. At the same impact height, the variation of resistance under the standard impactor testing was less than that under the knife impactor. Taking the impact height of around 1000 mm as an example, for the standard impactor, there were no significant breakages of the fibers occurred and the resistance change was smaller than 6.0 kΩ. Nevertheless, for the knife impactor, the deeper displacement of fabrics resulted in the larger destruction of conductive electric channels. The resistance change increased up to 17.0 kΩ, which signified that the resistance change was also able to detect failure degree of composites.

Further, by comparing the resistance change under different impact heights, the variation amplitude of the electrical resistance increased with the growth of impact heights for both standard impactor and knife impactor. The higher released height corresponded to the larger gravitational potential energy of the impactor, thus the impact kinetic energy loaded on the surface of the fabrics became larger. Hence, it was meaningful to discover the relationships between the imapct energy and resistance variation during the impact process. It was shown in Fig. S3 a,b that there was an admirable linear relationship between impact kinetic energy and resistance variation for standard impactor (R^2 = 0.94) and knife impactor (R^2 = 0.99). In this case, the c-STG/Kevlar could dynamically sense the external impact energy, which indicated the c-STG/Kevlar fabrics possessed a wonderful mechano-electric performance toward dynamic sensors.

Secondly, in the high-velocity ballistic impact experiment, the electric resistance signals of both monolayer non-penetration and complete penetration samples were compared. The FSP could not completely penetrate the specimen at the initial velocity of 58.2 m/s (Fig. S4). The non-penetration initial velocity was lower than the ballistic limit velocity v_{bl}, which further verified the rationality of Recht-Ipson fitting equation. In the non-penetration situation, the resistance variation of the S11 c-STG/Kevlar was 48.0 kΩ. Nevertheless, as shown in Fig. 9c, once the initial velocity reached to 113.7 m/s, the electrical resistance also remained almost constant before penetrating (state I). Then, as soon as the FSP contacted and completely penetrated the sample (state II), a larger resistance change of 78.3 kΩ suddenly occurred comparing to the non-penetration sample. The apparent distinctions in the resistance change corresponded to the damage degree. Finally, the resistance rapidly decreased after the end of the contacting process between the FSP and fabrics (state III). Therefore, the conductive carbon black particles in the STG/Kevlar system made it possible to dynamically capture the degree of the external loadings.

The mechano-electric performance of c-STG/Kevlar could be explained by evolutions in the structure of the conductive network under external loading. During the preparation process of the c-STG/Kevlar, the conductive particles were well dispersed in STG. As the external force loaded on the c-STG/Kevlar composites, the macroscopic shear thickening property of fabrics materials was derived from the destruction of the cleavage “B–O” dynamic-bond [37] in the microcosmic level (Fig. 10a). The conductive networks were also destroyed with the destruction of the “B–O” dynamic-bond, leading to the growth of resistance. The larger of the external loading, the more obvious damage of the conductive networks appeared (Fig. 10 b-d), the red part in Fig. 10 represented the interdict of conductive networks, resulted in an increase of the resistance. Nevertheless, the “B–O” dynamic-bond in the STG possessed the ability of self-healing and the conductive networks reorganized with the recombination of “B–O” cross-link corresponding to the resistance recovery process in the unloading process [38]. Therefore, the unique characteristics of “B–O” dynamic-bond played an important role in the mechano-electric performance.

3.4. Application of c-STG/Kevlar soft fabrics

Based on the anti-impact property and mechano-electric coupling performance, a novel helmet was manufactured by attaching the 5-layer c-STG/Kevlar S11 fabrics on the surface of a helmet (Fig. 11a). The resistance response under an *in situ* hammer impact was analyzed qualitatively to further prove the reliability in practical applications (Fig. 11b). The resistance of the helmet maitained almost 2.0 kΩ without external loading. When the slight impact acted on the helmet, the resistance increased instantaneously as soon as the hammer contacted the samples (Fig. 11c). Once the loading was removed, the resistance of the helmet recovered to the initial level. 5 cycles of loading and unloading were conducted and it was found the resistance of the helmet was stably cycled. Next, with increasing of the impact energy, it was found that the electrical resistance variation of the helmet grew accordingly. The phenomenon was consistent with the low-velocity drop tower mechano-electric testings. Analogously, once the heavy

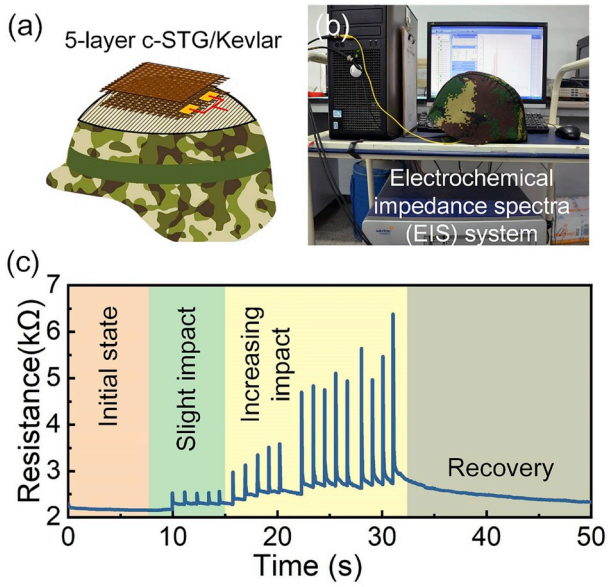

Fig. 11. (a) The schematic of c-STG Kevlar helmet; (b) the image of application testing device; (c) the curve of resistance signals of the application c-STG/Kevlar helmet under hammer impact.

loading was removed from the helmet, the resistance could quickly reduce to the initial level in 20 s and the c-STG/Kevlar fabrics helmet possessed the excellet stability in multiple damage monitoring. Hence, the combination performances of safeguarding, recoverable dynamic monitoring, the c-STG/Kevlar has broad potential in next generation wearable devices.

4. Conclusion

In this paper, a novel c-STG-Kevlar soft safeguarding composite was fabricated by impregnating c-STG into the Kevlar fabrics. The optimum component of the c-STG/Kevlar was designed and both the low-velocity drop tower testings and high-velocity ballistic experiments verified the carbon black and STG improved the anti-impact performance. The conductive carbon black endowed the c-STG/Kevlar with interesting mechano-electric coupling behavior and the resistance variation showed a good linear relationship to the impact energy. Owing to the outstanding mechano-electric performance, the variation in electic resistance of the c-STG/Kevlar could apply to monitor the amount of impact energy and the destruction degree. Finally, an impact-sensitive helmet attached with c-STG/Kevlar was constructed and it showed excellent sensitivity. As a result, the c-STG/Kevlar was believed to possess a wide potential for monitoring dynamic force in the next generation safe guarding body armor materials.

Acknowledgment

Financial supports from the National Natural Science Foundation of China (Grant No. 11822209,11772320), the Strategic Priority Research Program of Chinses Academy of Sciences (Grant No. XDB22040502), and the Fundamental Research Funds for the Central Universities (WK2090050045) are gratefully acknowledged. This study was also supported by the Collaborative Innovation Center of Suzhou Nano Science and Technology.

Appendix A. Supplementary data

Supplementary data to this article can be found online at https://doi.org/10.1016/j.compscitech.2019.107782.

References

[1] H. Palleti, S. Gurusamy, S. Kumar, R. Soni, B. John, R. Vaidya, A. Bhoge, N.K. Naik, Ballistic impact performance of metallic targets, Mater. Des. 39 (2012) 253–263.
[2] A.K. Jha, N. Shiresha, S. Murty, V. Diwakar, K. SreeKumar, Ballistic impact testing of AA2219 aluminium alloy welded plates and their metallurgical characterisation, Indian J. Eng. Mater. Sci. 12 (3) (2005) 221–226.
[3] J. Jiusti, E.H. Kammer, L. Neckel, N.J. Loh, W. Trindade, A.O. Silva, O.R.K. Montedo, A. De Noni, Ballistic performance of Al_2O_3 mosaic armors with gap-filling materials, Ceram. Int. 43 (2) (2017) 2697–2704.
[4] Z.H. Tan, X. Han, W. Zhang, S.H. Luo, An investigation on failure mechanisms of ceramic/metal armour subjected to the impact of tungsten projectile, Int. J. Impact Eng. 37 (12) (2010) 1162–1169.
[5] B. Matchen, Applications of ceramics in armor products, in: H. Mostaghaci (Ed.), Advanced Ceramic Materials: Applications of Advanced Materials in a High-Tech Society I1996, pp. 333-342.
[6] M. Grujicic, B. Pandurangan, D.C. Angstadt, K.L. Koudela, B.A. Cheeseman, Ballistic-performance optimization of a hybrid carbon-nanotube/E-glass reinforced poly-vinyl-ester-epoxy-matrix composite armor, J. Mater. Sci. 42 (14) (2007) 5347–5359.
[7] M. Hudspeth, A. Agarwal, B. Andrews, B. Claus, F. Hai, C. Funnell, J. Zheng, W.N. Chen, Degradation of yarns recovered from soft-armor targets subjected to multiple ballistic impacts, Composites Part A-Appl. S. 58 (2014) 98–106.
[8] A.K. Bandaru, V.V. Chavan, S. Ahmad, R. Alagirusamy, N. Bhatnagar, Ballistic impact response of Kevlar® reinforced thermoplastic composite armors, Int. J. Impact Eng. 89 (2016) 1–13.
[9] M.G. Dobb, D.J. Johnson, B.P. Saville, Supramolecular structure of a high-modulus polyaromatic fiber (Kevlar 49), J. Polym. Sci., Polym. Phys. Ed. 15 (12) (1977) 2201–2211.
[10] A. Manero, J. Gibson, G. Freihofer, J.H. Gou, S. Raghavan, Evaluating the effect of nano-particle additives in Kevlar (R) 29 impact resistant composites, Compos. Sci. Technol. 116 (2015) 41–49.
[11] M.H. Malakooti, H.S. Hwang, N.C. Goulbourne, H.A. Sodano, Role of ZnO nanowire arrays on the impact response of aramid fabrics, Compos. B Eng. 127 (2017) 222–231.
[12] S. Yang, V.B. Chalivendra, Y.K. Kim, Fracture and impact characterization of novel auxetic Kevlar®/Epoxy laminated composites, Compos. Struct. 168 (2017) 120–129.
[13] J. Qin, G. Zhang, L. Zhou, J. Li, X. Shi, Dynamic/quasi-static stab-resistance and mechanical properties of soft body armour composites constructed from Kevlar fabrics and shear thickening fluids, RSC Adv. 7 (63) (2017) 39803–39813.
[14] E. Brown, N.A. Forman, C.S. Orellana, H. Zhang, B.W. Maynor, D.E. Betts, J.M. DeSimone, H.M. Jaeger, Generality of shear thickening in dense suspensions, Nat. Mater. 9 (3) (2010) 220–224.
[15] M.M. Denn, J.F. Morris, D. Bonn, Shear thickening in concentrated suspensions of smooth spheres in Newtonian suspending fluids, Soft Matter 14 (2) (2018) 170–184.
[16] J. Lee, Z. Jiang, J. Wang, A.R. Sandy, S. Narayanan, X.-M. Lin, Unraveling the role of order-to-disorder transition in shear thickening suspensions, Phys. Rev. Lett. 120 (2) (2018) 028002.
[17] Y.S. Lee, E.D. Wetzel, N.J. Wagner, The ballistic impact characteristics of Kevlar® woven fabrics impregnated with a colloidal shear thickening fluid, J. Mater. Sci. 38 (13) (2003) 2825–2833.
[18] Z.H. Tan, W.H. Li, W. Huang, The effect of graphene on the yarn pull-out force and ballistic performance of Kevlar fabrics impregnated with shear thickening fluids, Smart Mater. Struct. 27 (7) (2018) 075048.
[19] A. Khodadadi, G.H. Liaghat, A.R. Sabet, H. Hadavinia, A. Aboutorabi, O. Razmkhah, M. Akbari, M. Tahmasebi, Experimental and numerical analysis of penetration into Kevlar fabric impregnated with shear thickening fluid, J. Thermoplast. Compos. Mater. 31 (3) (2018) 392–407.
[20] S. Gurgen, M.C. Kushan, W.H. Li, Shear thickening fluids in protective applications: a review, Prog. Polym. Sci. 75 (2017) 48–72.
[21] Z.H. Tan, L. Zuo, W.H. Li, L.S. Liu, P.C. Zhai, Dynamic response of symmetrical and asymmetrical sandwich plates with shear thickening fluid core subjected to penetration loading, Mater. Des. 94 (2016) 105–110.
[22] X.Y. Feng, S.K. Li, Y. Wang, Y.C. Wang, J.X. Liu, Effects of different silica particles on quasi-static stab resistant properties of fabrics impregnated with shear thickening fluids, Mater. Des. 64 (2014) 456–461.
[23] A.N. Dickson, J.N. Barry, K.A. McDonnell, D.P. Dowling, Fabrication of continuous carbon, glass and Kevlar fibre reinforced polymer composites using additive manufacturing, Addit. Manuf. 16 (2017) 146–152.
[24] S.S. Cao, Q. Chen, Y.P. Wang, S.H. Xuan, W.Q. Jiang, X.L. Gong, High strain-rate dynamic mechanical properties of Kevlar fabrics impregnated with shear thickening fluid, Composites Part A-Appl. S. 100 (2017) 161–169.
[25] Y. Park, Y. Kim, A.H. Baluch, C.G. Kim, Empirical study of the high velocity impact energy absorption characteristics of shear thickening fluid (STF) impregnated Kevlar fabric, Int. J. Impact Eng. 72 (2014) 67–74.
[26] Y. Kim, Y. Park, J. Cha, V.A. Ankem, C.G. Kim, Behavior of Shear Thickening Fluid (STF) impregnated fabric composite rear wall under hypervelocity impact, Compos. Struct. 204 (2018) 52–62.
[27] Z.H. Tan, J.H. Ge, H. Zhang, P.C. Zhai, W.H. Li, Dynamic response of shear thickening fluid reinforced with SiC nanowires under high strain rates, Appl. Phys. Lett. 111 (3) (2017) 031902.
[28] Q.Y. He, S.S. Cao, Y.P. Wang, S.H. Xuan, P.F. Wang, X.L. Gong, Impact resistance of shear thickening fluid/Kevlar composite treated with shear-stiffening gel, Composites Part A-Appl. S. 106 (2018) 82–90.

[29] C.H. Xu, Y. Wang, J. Wu, S.C. Song, S.S. Cao, S.H. Xuan, W.Q. Jiang, X.L. Gong, Anti-impact response of Kevlar sandwich structure with silly putty core, Compos. Sci. Technol. 153 (2017) 168–177.
[30] H.X. Deng, Y. Du, Z.M. Wang, J.C. Ye, J. Zhang, M.C. Ma, X. Zhong, Poly- stable energy harvesting based on synergetic multistable vibration, Commun. Phys. 2 (1) (2019) 21.
[31] B. Fugetsu, E. Sano, H.W. Yu, K. Mori, T. Tanaka, Graphene oxide as dyestuffs for the creation of electrically conductive fabrics, Carbon 48 (12) (2010) 3340–3345.
[32] W.H. Kim, J.H. Park, S. Kaluvan, Y.S. Lee, S.B. Choi, A novel type of tunable magnetorheological dampers operated by permanent magnets, Sensor. Actuat. A-Phys. 255 (2017) 104–117.
[33] C.S. Boland, U. Khan, G. Ryan, S. Barwich, R. Charifou, A. Harvey, C. Backes, Z. Li, M.S. Ferreira, M.E. Mobius, R.J. Young, J.N. Coleman, Sensitive electromechanical sensors using viscoelastic graphene-polymer nanocomposites, Science 354 (6317) (2016) 1257–1260.
[34] S.S. Zhang, S. Wang, Y.P. Wang, X.W. Fan, L. Ding, S.H. Xuan, X.L. Gong, Conductive shear thickening gel/polyurethane sponge: a flexible human motion detection sensor with excellent safeguarding performance, Composites Part A-Appl. S. 112 (2018) 197–206.
[35] S. Wang, S.H. Xuan, M. Liu, L.F. Bai, S.S. Zhang, M. Sang, W.Q. Jiang, X.L. Gong, Smart wearable Kevlar-based safeguarding electronic textile with excellent sensing performance, Soft Matter 13 (13) (2017) 2483–2491.
[36] R.F. Recht, T.W. Ipson, Ballistic perforation dynamics, J Appl. Mech-T ASME 30 (3) (1963) 1–7.
[37] S. Kutanis, M. Karakisla, U. Akbulut, M. Sacak, The conductive polyaniline/poly (ethylene terephthalate) composite fabrics, Composites Part A-Appl. S. 38 (2) (2007) 609–614.
[38] Y.P. Wang, L. Ding, C.Y. Zhao, S. Wang, S.H. Xuan, H. Jiang, X.L. Gong, A novel magnetorheological shear-stiffening elastomer with self-healing ability, Compos. Sci. Technol. 168 (2018) 303–311.